frontiers | Frontiers in Marine Science

TYPE Original Research
PUBLISHED 14 April 2023
DOI 10.3389/fmars.2023.1083233

OPEN ACCESS

EDITED BY
Selvaraj Kandasamy,
Xiamen University, China

REVIEWED BY
Yanguang Liu,
Ministry of Natural Resources, China
Rebecca A Pickering,
Lund University, Sweden

*CORRESPONDENCE
Su Mei Liu
sumeiliu@ouc.edu.cn

SPECIALTY SECTION
This article was submitted to Marine Biogeochemistry, a section of the journal Frontiers in Marine Science

RECEIVED 28 October 2022
ACCEPTED 23 March 2023
PUBLISHED 14 April 2023

CITATION
Ma Y, Yang B, Zhou N, Huang J, Liu SM, Zhu D and Liang W (2023) Distribution and dissolution kinetics of biogenic silica in sediments of the northern South China Sea. *Front. Mar. Sci.* 10:1083233. doi: 10.3389/fmars.2023.1083233

Distribution and dissolution kinetics of biogenic silica in sediments of the northern South China Sea

Yuwei Ma [1,2], Bin Yang [3], Nan Zhou [1,2], Jin Huang [4,5], Su Mei Liu [1,2]*, Dongdong Zhu [1,2,6] and Wen Liang [1,2]

[1]Frontiers Science Center for Deep Ocean Multispheres and Earth System, and Key Laboratory of Marine Chemistry Theory and Technology, Ministry of Education, Ocean University of China, Qingdao, China, [2]Laboratory for Marine Ecology and Environmental Science, Qingdao National Laboratory for Marine Science and Technology, Qingdao, China, [3]Guangxi Key Laboratory of Marine Environmental Change and Disaster in Beibu Gulf, Beibu Gulf University, Qinzhou, China, [4]College of Chemistry, Chemical Engineering and Resource Utilization, Key Laboratory of Forest Plant Ecology Ministry of Education, Northeast Forestry University, Harbin, China, [5]School of Forestry, Northeast Forestry University, Harbin, China, [6]University of Brest, Centre national de la recherche scientifique (CNRS), L'Institut de recherche pour le développement (IRD), Ifremer, Institut Universitaire Européen de la Mer, Plouzané, France

The dissolution efficiency of sedssimentary biogenic silica ($bSiO_2$) dramatically affects the regeneration of dissolved silicic acid (dSi) at the sediment-water interface, which is a crucial pathway to maintain Si balance and silicic productivity growth in marine environments. We conducted wet alkaline leach and flow-through experiments to explore the dissolution behaviors of sedimentary $bSiO_2$ in the northern South China Sea (NSCS), one of the largest marginal sea continental shelves. The $bSiO_2$ contents of surface sediments were 0.64 - 2.06%, with an average of 1.04 ± 0.35%, varying with isobath water depth. The solubility of $bSiO_2$ in surface sediments ranged from 227 μmol L^{-1} to 519 μmol L^{-1}, and the dissolution rate constants varied from 0.67 to 1.53 yr^{-1} under specific conditions in lab incubation. The correlation between the biogenic materials ($bSiO_2$, OC, and TN) revealed a different preservation pattern of $bSiO_2$ in finer ($\Phi > \sim 5.5$) and coarser ($\Phi < \sim 5.5$) sediments. The high concentration of Al in sea water and "Al – detrital – $bSiO_2$" interactions in sediments significantly interfered with the apparent solubility and dissolution dynamics of $bSiO_2$. We combined the regional characteristics (primary production, bottom current, and resuspension-deposition) and the reconstructed dissolution kinetics of $bSiO_2$ explained the mismatch between the surface (diatom biomass)/(total phytoplankton biomass) ratio and the sedimentary $bSiO_2$/OC ratio, and the mismatch between the surface $bSiO_2$ primary productivity and the $bSiO_2$ sediment records in the NSCS. The resuspension-deposition, the higher reconstructed rate constants (0.94 ± 0.13 yr^{-1}), and the dissolution rate (0.20 ± 0.01 yr^{-1}) were responsible for the lower $bSiO_2$/OC ratio (0.45 ± 0.28) at the inner shelf, and the winnowing process at the outer shelf with the lower reconstructed reactivity (0.30 yr^{-1}) and dissolution rate (0.001 yr^{-1}) led to the good preservation of $bSiO_2$ in the upper

slope. Furthermore, through the comparison with other sea areas, the relatively lower reactivity (1.12 ± 0.3 yr^{-1}) of $bSiO_2$ in sediments supported the notion that the NSCS sediments may serve as an important silica sink in the world ocean silica cycle.

KEYWORDS

biogenic silica, dissolution, detrital, aluminum, silicon cycle, Northern South China Sea

1 Introduction

Biogenic silica ($bSiO_2$) is one of the most important components in marine sediments and believed to be a potentially powerful proxy to reconstruct paleoproductivity (Mortlock et al., 1991; Ragueneau et al., 2000). Diatoms are the dominant siliceous producers and responsible for nearly half of the oceanic uptake of CO_2 from the atmosphere (Nelson et al., 1995). Thus, the intimate coupling between the Si and C cycles have driven substantial studies in the last few decades in order to better understand the biogeochemical cycle of Si in marine systems (DeMaster et al., 1996; Nelson et al., 1996; Sayles et al., 2001; Ragueneau et al., 2006; Krause et al., 2011).

The idealized "silica pump", put forward by Dugdale et al. (1995), described a less efficient recycling of $bSiO_2$ than particulate organic matter in the euphotic zone, leading to more efficient export of $bSiO_2$ from upper to deep oceans and the potential limitation of dSi in a diatom-dominated system. Diatom frustules are readily dissolved in strongly undersaturated seawater when organisms die, and the "silica pump" efficiency largely depends on dissolution of $bSiO_2$ before it can be exported to the upper mixed layer in variable marine settings (Brzezinski and Nelson, 1989; Brzezinski and Nelson, 1995; Nelson et al., 1995; Nelson and Dortch, 1996; Bidle et al., 2003). Therefore, the dissolution of $bSiO_2$ is a vital process controlling the marine Si biogeochemical cycle. Particularly in sediments, ~ 89% of deposited $bSiO_2$ is regenerated back through dissolution and other processes (i.e., diffusion, advection, bioturbation, or bioirrigation) on a global ocean scale, which is an important channel to maintain silicic acid (dSi) in a relative steady state in surface oceans by diffusion and/or upwellings for silicic productivity growth (DeMaster, 2002; Tréguer et al., 2021). A considerable number of researches have been inspired to not only explore the temporal and spatial variability of sedimentary $bSiO_2$ dissolution kinetics in variable settings in open oceans (Hurd, 1973; Kamatani et al., 1988; Van Cappellen, 1996; Van Cappellen and Qiu, 1997a; Van Cappellen and Qiu, 1997b; Dixit et al., 2001; Ragueneau et al., 2001; Gallinari et al., 2002; Van Cappellen et al., 2002; Khalil et al., 2007; Gallinari et al., 2008; Cheng et al., 2009) and marginal seas (Van Bennekom et al., 1991; Rickert, 2000; Rickert et al., 2002; Gallinari et al., 2008; Wu et al., 2017; Wu and Liu, 2020), but also the factors ultimately controlling the fate of sedimentary Si, including ambient physical factors such as temperature (Lawson et al., 1978; Kamatani and Riley, 1979; Van Cappellen and Qiu, 1997a; Van Cappellen and Qiu, 1997b), pressure (Willey, 1974; Loucaides et al., 2012), pH (Van Cappellen and Qiu, 1997a; Van Cappellen and Qiu, 1997b; Loucaides et al., 2008), salinity (Loucaides et al., 2008), ionic composition (Loucaides et al., 2008), and its intrinsic nature such as surface chemical properties (Dixit and Van Cappellen, 2002; Fraysse et al., 2006; Loucaides et al., 2012), silicious organism species, and silicification degree (Loucaides et al., 2012). In addition, Rickert et al. (2002) addressed the removal of organic or inorganic coatings (that protect diatom frustules from dissolution by avoiding direct contact with seawater) will enhance the reactivity by at least an order of magnitude. Thus, the roles of aggregation, fecal pellets, or grazing must be considered (Moriceau et al., 2007). Bacterial ectoprotease action on marine diatom detritus strongly accelerates silica dissolution rates by removing the organic coating (Bidle and Azam, 1999; Bidle and Azam, 2001; Bidle et al., 2003), which also plays a significant role in regulating the "silica pump" and sedimentary $bSiO_2$. In addition, the interaction between Al (or K, Li, Na, Mg, Fe, and other reactive elements in porewater) and $bSiO_2$ during early diagenesis have been proposed as a special pathway to form authigenic clay, and have a profound impact on the burial of marine $bSiO_2$ (Rahman et al., 2017; Tréguer et al., 2021), especially in marginal seas with large estuaries (Michalopoulos and Aller, 2004).

The northern South China Sea (NSCS) is a semi-closed marginal sea with a broad shallow water shelf in the Western Pacific Ocean, and features relatively strong biological activity induced by river discharge, seasonal coastal upwelling, and monsoon winds (Chen et al., 2006; Hung et al., 2007). Accordingly, significant seasonal and spatial changes of primary production (Ning et al., 2004; Chen, 2005), particulate organic matter (Ho et al., 2010; Cai et al., 2015), and phytoplankton community structure (Cai et al., 2015) occurs in the NSCS. The second largest river in China, the Pearl River, empties an average freshwater discharge of 482 km^3 yr^{-1} and sediment load of 96 Mt yr^{-1} carrying ~ 53 Gmol-Si yr^{-1} into the NSCS (Liu et al., 2009; Ma et al., 2022), which results in relatively eutrophic conditions. These are benefits for the growth of micro-phytoplankton (> 20 μM in size), such as diatoms, which account for > 75% of the Chl-a concentration in NSCS coastal waters (Xiao et al., 2018). Large terrigenous input and oceanic current system lead to a complex sediments composition and transportation process. (Liu et al., 2016). All of these factors have a significant consequence on the "silica pump" and sedimentary $bSiO_2$. However, prior research on

sedimentary $bSiO_2$ in the South China Sea has mainly focused on distribution features (Zhou et al., 2010; Liu et al., 2012; Zhang et al., 2015) or burial fluxes (Ma et al., 2022). The dissolution and preservation mechanisms of sedimentary $bSiO_2$ is missing in this region. Here, we report the results of flow-through experiments using samples with different sediment components to study the characters influencing factors of the $bSiO_2$ dissolution and the implications for $bSiO_2$ preservation in the NSCS.

2 Materials and methods

2.1 Sample collection

Sampling expeditions were executed in the NSCS onboard the R/V "*Shi Yan 3*" during March and April 2014. In total, 40 surface sediment samples (0 – 2 cm) were collected using a stainless-steel box sampler. The sampling locations are indicated in Figure 1A. The collected sediments were sealed in polyethylene Ziploc bags, and the air removed at the same time. Then, they were immediately frozen at - 20 °C until further processing in the laboratory. Note that our sampling sites were mainly located in the northern continental shelf area of the South China Sea, and a few stations (i.e., 7, 8, 21, 34, and 88) were located in the NSCS shelf-break area (Figure 1A). A conductivity temperature depth (CTD) system was used to measure the bottom water temperature, salinity, and depth.

2.2 Flow-through experiments

Apparent solubility and dissolution kinetics of $bSiO_2$ of eight surface sediments with different sediment components (Figure 1A; Table 1) in the NSCS were measured using stirred flow-through reactors (Figure 2) (Van Cappellen and Qiu, 1997a; Gallinari et al., 2002; Rickert et al., 2002; Gallinari et al., 2008). Each reactor consisted of a cell with a suspended Teflon-coated magnetic stirring bar at the bottom, with a volume of 50 cm^3. Both cell ends were closed by nylon filters with a pore size of 0.45 μm, and the filters were supported by PTFE grids. The filters and grids were held in place by screw-on caps. The flowing solution could be pumped in or out of the headspaces without a barrier through narrow channels of the caps. The well-closed flow-through reactors sat on top of a multipoint magnetic stirrer, which were put into an accurately temperature-controlled incubator. All parts of the system were interconnected with PTFE pipes. In the experiments, up to 2 g of homogenized sediment sample with no pretreatment were added to the reactor (25°C) and an input solution of a well-characterized composition (0.7 M NaCl, buffered at pH 8.0 ± 0.1 using bicarbonate, with known different dSi concentrations) was pumped through the reactor at a constant flow rate until the dSi concentration in the reactor outflow stabilized. Because of the relatively low contents of $bSiO_2$ in the NSCS, the flow rates were maintained between 0.8 - 3.1 ml/h to ensure a measurable difference of dSi concentration between the inflow and outflow due to dissolution or precipitation. Lower flow rates were under higher degrees of undersaturation. The dSi concentration in the input solution was progressively decreased to produce a transition from a precipitation to a dissolution regime. In general, a group of experiments lasted 10 - 18 days according to flow rate and time to reach the steady-state. The dSi concentration and pH in the input solution were monitored throughout the whole course to ensure no influential fluctuations. All of the experiments were carried out under

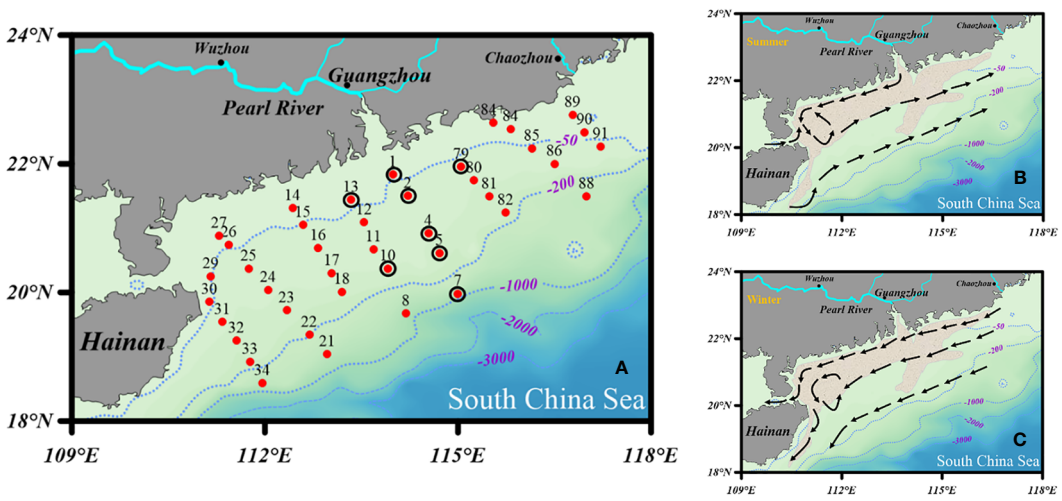

FIGURE 1
Sampling sites and patterns of surface coastal currents in **(B)** summer and **(C)** winter [modified from Wei et al. (2020)]. The khaki-shaded area represents the distribution of the Pearl River-derived mud belt based on Ge et al. (2014). The sediment samples were collected in April 2014. The red dots (*) and black circles (○) in **(A)** represent the grid stations and sediment locations for the flow-through experiments.

10.3389/fmars.2023.1083233

TABLE 1 Characterization of the sediment samples used for flow-through experiments.

Station	Depth (m)	Temperature (°C)	Sediment type[a]	SSA[b] (m^2/g)	Mean grain size (Φ)	$bSiO_2$ (%)	Organic matter[c] (%)	$CaCO_3$ (%)	Detritus[d] (%)
1	40	20.14	Clay - silt	11.634	6.52	1.23	2.58	3.4	92.8
2	54	19.46	Sand - silt	7.088	5.35	0.94	1.34	7.9	89.8
4	81	19.93	Silt - sand	2.280	3.42	0.64	0.78	9.6	89.0
5	107	18.62	Silt - sand	2.106	3.93	0.73	0.64	12.6	86.1
7	733	6.38	Silt	12.439	6.72	2.06	2.63	21.5	73.8
10	99	19.59	Silt - sand	–	6.91	0.7	0.64	13.5	85.2
13	36	20.51	Clay - silt	–	3.51	1.69	2.88	5.6	89.8
79	61	21.35	Sand - silt	–	5.86	1.4	2.27	4.9	91.4

[a]Shepard sediment classification.
[b]BET specific surface area.
[c]Assumes Redfield composition [Organic matter (%) = 2.8 × OC (%)] (Sayles et al., 2001).
[d]Detritus was the sample's remaining mineral percentage, including authigenic aluminosilicates, once $CaCO_3$, organic matter, and $bSiO_2$. Contents were extracted (Rickert et al., 2002).
"-" means no data.

ambient atmospheric pressure and sustained for about 80 days. It is worth noting that the homogeneous process perhaps enhances the reactivity of $bSiO_2$ by crushing the silicate minerals in the flow-through experiment like in wet alkaline digestion (DeMaster et al., 1983; Ward et al., 2021). Van Cappellen and Qiu (1997a) were the first to introduce flow-through experiments into the study of $bSiO_2$ dissolution in the Southern Ocean, however, the numerously subsequent studies followed the homogeneous process and not well quantified this influencing factor yet (Gallinari et al., 2002; Loucaides et al., 2008; Wu et al., 2017). Regardless, the sediment homogeneous process remains a commonly used method of sample preparation and we followed this procedure.

2.2.1 Solubility measurements

The reaction rate of $bSiO_2$ in various inflow solutions were calculated from the difference between each input dSi concentration and the corresponding steady-state output dSi concentration (Rickert et al., 2002):

$$R = \frac{V * \Delta[Si]}{m_{bSiO_2}} \quad (1)$$

where R (μmol g^{-1} h^{-1}) represents the reaction rate of $bSiO_2$; V (ml h^{-1}) donates the volume of flow rate; $\Delta[Si]$ (μmol L^{-1}) is the difference between outflow and inflow solution of concentration of dSi ($\Delta[Si] = [Si_{out}] - [Si_{in}]$); m_{bSiO_2} . (represents the mass of extractable $bSiO_2$ within the reactor. A positive rate indicates the dSi is undersaturated (dissolution) in the reactor, and a negative rate reflects oversaturation (precipitation). The solubility was estimated by linearly interpolating the two closest points from the equilibrium to obtain the value at which there was neither dissolution nor precipitation ($[Si_{out}] = [Si_{in}]$, or $R = 0$).

2.2.2 Dissolution rate constant and reaction order measurements

The flow-through reactor technique is particularly suitable for studying reaction kinetics as a function of the departure from equilibrium, which can provide important information

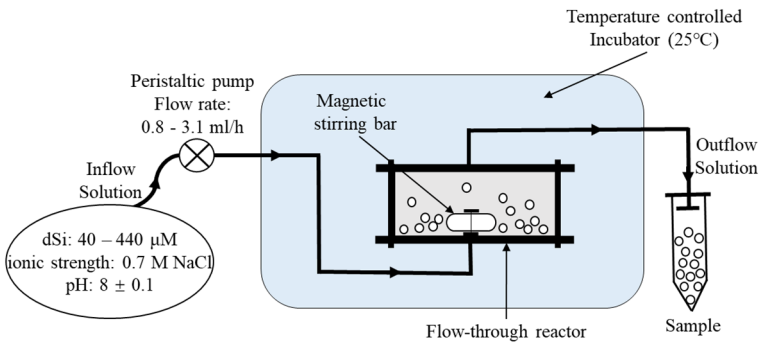

FIGURE 2
Schematic illustration of continuous flow-through experiments. Inflow solution with different dSi concentrations and given conditions were added to the reactor by a flow rate controlled peristaltic pump. PTFE pipes were used for interconnecting all parts of the system.

concerning the reactivity of the $bSiO_2$ (Van Cappellen, 1996; Gallinari et al., 2008). The non-linear dissolution kinetics law was proposed by several studies to model the experimental data (Van Cappellen and Qiu, 1997a; Van Cappellen and Qiu, 1997b; Rickert et al., 2002; Gallinari et al., 2008):

$$R = k_{diss}\left(1 - \frac{[Si]}{[Si]_{eq}}\right)^{m} \quad (2)$$

Here, R (μmol g^{-1} h^{-1}) is the reaction rate of $bSiO_2$; k_{diss} (μmol g^{-1} h^{-1}) donates the dissolution rate constant of $bSiO_2$, which reflect the apparent reactivity of the $bSiO_2$ particles; $[Si]$ (μM) is the dSi concentration; $[Si]_{eq}$ (μM) represents the apparent solubility of $bSiO_2$, and m is the reaction order that indicates the extent of deviation from the linear dissolution dynamics of $bSiO_2$.

2.3 Measurements of sedimentary $bSiO_2$, organic carbon, total nitrogen, and calcium carbonate

Sediment samples were freeze-dried in the laboratory. It is noteworthy that the grinding effect on the measurement of $bSiO_2$ by wet alkaline digestion could enhance the calculated $bSiO_2$ concentrations up to ~50% (DeMaster et al., 1983; Ward et al., 2021). Therefore, to improve the measurement reproducibility (< 2%) in low $bSiO_2$ content samples from marginal seas, the sediments were as gently as possible ground using an agate pestle and mortar (trying to avoid crushing the silicious structures and silicate minerals) for homogenization. The sedimentary $bSiO_2$ contents were analyzed using a modified alkaline leaching method (Liu et al., 2002) which combined the methods described in DeMaster (1981) and Mortlock and Froelich (1989). In detail, ~ 100 mg sediment samples were placed in 50 ml polypropylene centrifuge tubes after removing organics and carbonates with H_2O_2 and HCl. Exactly 40 ml of 2% Na_2CO_3 solution was added to the samples. The tubes were covered tightly and mixed homogenously using a vortex rotating machine, then incubated in a water bath preheated to 85 °C. After 1 h, the tubes were removed and centrifuged. Then, 125 μl of clear centrifugation supernatant was pipetted from each extraction solution for dSi analysis. This procedure was repeated for 1 – 8 h. Note that after each sampling, the tubes were stirred vigorously to resuspend the sediment then placed again in the water bath. All sampling steps were completed quickly to minimize dSi loss on solid surfaces. The concentrations of dSi in the leaching solution were determined using the molybdate blue spectrophotometric method (Mortlock and Froelich, 1989). The $bSiO_2$ content was calculated by a first order kinetic model, that is, the dSi we measured was a function of time t (Koning et al., 1997; Rickert et al., 2002):

$$[dSi\,\%]_t = [bSiO_2\,\%]_0 \times (1 - e^{-k_{Na_2CO_3}t}) + b_{Na_2CO_3}t \quad (3)$$

where $[bSiO_2\%]_0$ represents the content of $bSiO_2$ (wt.%) in the sediment sample; $[dSi\%]_t$ donates extracted content of SiO_2 at time t; $k_{Na_2CO_3}$. d $b_{Na_2CO_3}$. e apparent rate constants in Na_2CO_3 solution that summarize the influence of biogenic and detrital matrix on the dSi concentration, respectively (Koning et al., 1997; Rickert et al., 2002). The coefficient of variation (i.e., relative stand deviation) for five parallel extractions was< 2.00%, indicating good reproducibility. The result of inter-laboratory comparison through this method demonstrates good accuracy of $bSiO_2$ measurement (Liu et al., 2002; Wu et al., 2015).

The OC and TN contents were measured using a CHNOS Elemental Analyzer (Vario EL-III; Elementar Analysensysteme GmbH, Germany) after inorganic carbon was removed *via* acidification with 1 M HCl. The analytical precision of OC and TN was< 6% based on duplicate measurements (Liu et al., 2010). The data of OC contents have been published in Yang et al. (2018). The content of $CaCO_3$ was measured using acid-base titration (Müller, 1966), and the coefficient of variation was 1.0% for five parallel extractions. To calculate the detrital material contents, the OC was converted to organic matter contents assuming a multiplier of 2.8 g of organic matter per g of carbon (Redfield composition) (Sayles et al., 2001). Therefore, detritus % = 100 – ($bSiO_2$% + $CaCO_3$% + OC% × 2.8).

2.4 Specific surface area and grain size (Φ)

The specific surface area (SSA, m^2 g^{-1}) of the sediments were determined by the conventional N_2-BET method using an ASAP2460 full-automatic surface area analyzer (ASAP2460, Micromeritics, USA). Samples were heated overnight at 90 °C and for one hour at 150 °C prior to analysis. The multi-point BET surface area was calculated from the N_2 absorption isotherm. The sediment grain size was analyzed using a laser particle size analyzer (Mastersizer 2000; Malvern Instruments Ltd., Malvern, Worcestershire, UK) capable of analyzing grain sizes from 0.02 to 2000 μm. Three sediment size categories were distinguished: (1) clay: D< 4 μm; (2) silt: 4< D< 63 μm; and (3) sand: D > 63 μm. The samples were analyzed in duplicate, and the analytical precision was< 2%. The mean grain size was reported as Φ, where $\Phi = -\log_2 D$ (D unit: mm) (Krumbein, 1934). The data of grain size have been published in Yang et al. (2018).

3 Results

3.1 Distribution of biogenic ($bSiO_2$, OC, $CaCO_3$) matters and abiogenic detrital

The contents of $bSiO_2$ in surface sediments of the NSCS varied from 0.64% to 2.06%, with an average of 1.04% ± 0.35% (Figure 3A). As a whole, the $bSiO_2$ contents presented a strong zonal distribution tendency and varied with the water depth isobath, which decreased from the inner shelf (< 50 m) to the outer shelf (50 - 200 m), and then increased to the upper slope (> 200 m). Furthermore, higher levels were predominantly observed in the region with fine-grained (D< 63 μm) sediments and lower $bSiO_2$ concentrated in the sandy (D > 63 μm) sediments. The horizontal distribution of the OC

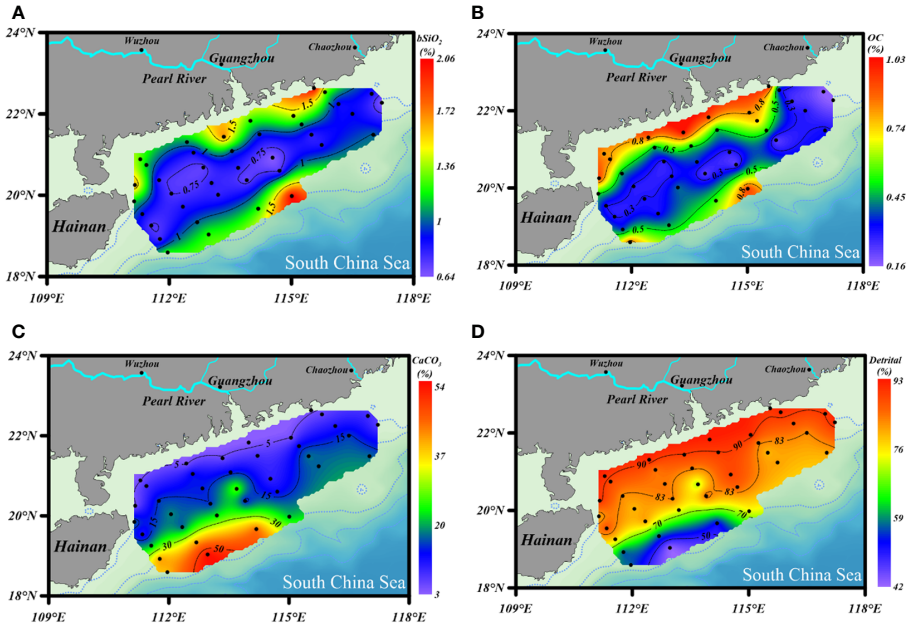

FIGURE 3
Distribution of **(A)** $bSiO_2$ (%), **(B)** OC (%), **(C)** $CaCO_3$ (%), and **(D)** detrital mineral (%) contents in surface sediments of the NSCS.

contents showed similar patterns with that of $bSiO_2$, which were 0.1% to 1.03%, with an average of 0.49% ± 0.27% (Figure 3B). The $bSiO_2$/OC mole ratios varied from 0.24 to 1.06, with lower values at the inner shelf (0.45 ± 0.28) and upper slope (0.42 ± 0.11) and higher values at the outer shelf (0.51 ± 0.14). The $CaCO_3$ and detrital contents were 16.6% ± 12.4% (3.4% - 54.8%) and 80.9% ± 12.4% (42.7% - 92.8%), respectively. The distribution trends of these two components were opposite, increasing gradually from the inner shelf to the upper slope for $CaCO_3$ and decreasing gradually for detritus (Figures 3C, D).

3.2 Apparent solubility and dissolution kinetics of $bSiO_2$

The dissolution rates of sedimentary $bSiO_2$ were plotted as a function of the outflow steady-state dSi concentrations (Figure 4). The uncertainties of the solubilities were calculated by the narrow fluctuation of $[Si_{out}]$ after steady state conditions were reached. The apparent solubility of $bSiO_2$ in surface sediments of the NSCS ranged from 227 to 519 μM with a mean value of 298 ± 94 μM, which is much lower than the solubility of the fresh diatom frustules (~ 1100, 0

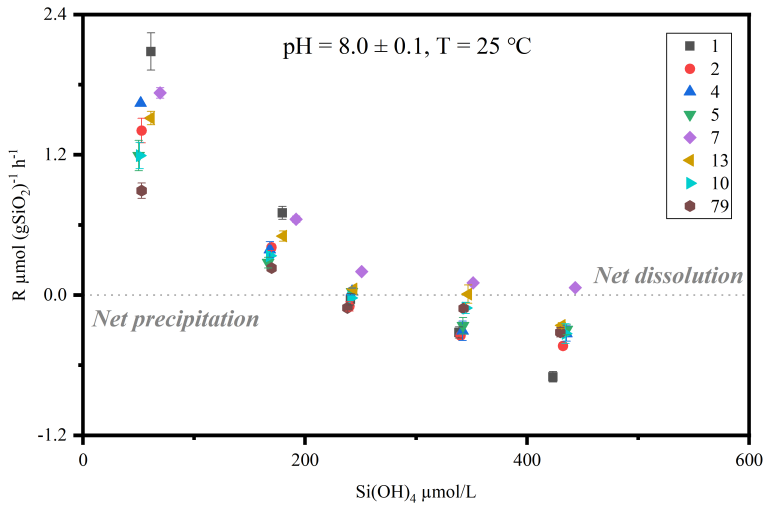

FIGURE 4
Steady state $bSiO_2$ dissolution-precipitation rates [μmol $(gSiO_2)^{-1}$ h^{-1}] are plotted as a function of dSi outflow concentrations (T = 25 °C, pH = 8.0 ± 0.1) in surface sediments of the NSCS. Positive rates indicate net dissolution, and negative rates indicate net precipitation. The legends and numbers in the upper right corner indicate different stations conducted flow-through experiments. The uncertainties are shown by error bars.

– 4 °C) (Hurd, 1973). In general, the solubility of the inner shelf and upper slope are higher than that of the outer shelf (except station 10). The highest solubility value was observed at station seven on the upper slope, where the $bSiO_2$ content was highest. The lowest value was recorded at station two on the outer shelf. The dissolution rate constant of the inner shelf and upper slope was higher than that of the outer shelf, which was from 0.67 to 1.53 yr^{-1}, with an average of 1.12 ± 0.3 yr^{-1} (Table 2). The east side (station 13) of the Pearl River estuary is evidently higher than the west side (station 79). Station one and 79 recorded the highest and lowest values, respectively. In addition, the reaction order (m >1) ranged from 1.1 to 3.42. A relative higher value was observed at station seven.

3.3 Grain size (Φ) and specific surface area character

The surface sediments in the NSCS were mainly composed of silt (4 - 63 μm) and sand (> 63 μm). Fine-grained sediments were found primarily in the Pearl River estuary and adjacent coastal region, and secondarily in the upper-slope area (station 7, 8, 21, and 34), whereas coarser sediments occurred mainly in the outer-shelf area (50 – 200 m), especially in the northeast (Figure 5). The highest values of specific surface area (SSA) were recorded at station one and seven, and the lowest values at station two, four, and five (Table 1).

4 Discussion

4.1 The distribution character of sedimentary $bSiO_2$

The distribution of $bSiO_2$ (Figure 3A) and $bSiO_2$/OC ratio (Figure 6) revealed a mismatch between the (diatom biomass)/(total phytoplankton biomass) ratio and the sedimentary $bSiO_2$/OC ratio at the inner shelf and outer shelf, and also a mismatch between the $bSiO_2$ primary productivity and the $bSiO_2$ sediment records at the upper slope of the NSCS. The sedimentary $bSiO_2$ record is believed to a good indicator for the surface $bSiO_2$ primary production (Schrader and Sorknes, 1991). The wide shelf of the NSCS receives a large discharge of terrigenous nutrients and results in overall enhanced biological productivity (Han et al., 2012). But the primary production presented distinct regional characteristics at the inner shelf (< 50 m), outer shelf (50 – 200 m), and upper slope (> 200 m). The satellite remote-sensed spatial distribution of Chl-a showed a gradient decrease from nearshore to offshore, and changes roughly along the 50 m isobath with concentrations of ~ 1 mg m^{-3} in all seasons. In addition, the total biomass of phytoplankton and the proportion of diatoms in the mixed layer also showed a gradient decrease from the nearshore to the offshore throughout the year (Xiao et al., 2018), which is consistent with the variation of surface primary productivity (< 40 m: 1.73 ± 0.12 g-C m^{-2} d^{-1}; 40 – 120 m: 0.67 ± 0.35 g-C m^{-2} d^{-1}; > 120 m: 0.43 ± 0.02 g-C m^{-2} d^{-1}) (Pan et al., 2015). This evidence indicated that even though there is no report of primary production of $bSiO_2$ in the NSCS at present, it can be speculated that the distribution of $bSiO_2$ primary production should be in a decreasing trend from nearshore to offshore. Therefore, the high sedimentary contents of $bSiO_2$ accumulated in the inner-shelf region (1.27% ± 0.39%) (Figure 3A) is mainly attributed to the enhanced $bSiO_2$ primary production by the large discharge of terrigenous nutrients, especially in the area affected by the perennial westward plume of the Pearl River (station 13). However, a mismatch between the $bSiO_2$ primary productivity and the $bSiO_2$ sediment records at the upper slope of the NSCS was observed. High contents of $bSiO_2$ (1.43% ± 0.42%) were recorded in the upper-slope region (0.71% ± 0.24%) (Figure 3A). It is obvious this was not related to the euphotic $bSiO_2$ primary production. Our flow-through experimental results showed a dissolution kinetics-controlled preservation of $bSiO_2$ in this area (discussed in section 4.4).

In addition to primary production, sediment grain size plays a role in the distribution of $bSiO_2$. As Figure 5 shows, the distribution of mean grain size (Φ) was similar with the distribution of $bSiO_2$ (%), and fine-grained sediments were mainly distributed in the inner-shelf and the upper-slope regions. The strong correlation between "Φ" values of mean grain size and $bSiO_2$ contents ($r = 0.71$, $p < 0.01$) indicated fine-textured particles (silt and clay) have greater physical protection for $bSiO_2$. Compared with different biogenic material (OC and TN) in different sediment types, we found a different preservation patterns of $bSiO_2$ in the sediments of the NSCS. As a

TABLE 2 Flow-through experimental results.

Station	Solubility (μmol/L)	k_{diss} 25°C (yr^{-1})	k_{diss} 25°C (μmol m^{-2} h^{-1})[a]	Situ-k_{diss} (yr^{-1})[b]	Situ-dSi Concentration[c]	Situ-dissolution rate [yr^{-1}][d]	Reaction order (m)
1	272 ± 6	1.53	0.25	1.02	191	0.21	1.32
2	227 ± 18	0.99	0.27	0.63	170	0.14	1.1
4	251 ± 1	1.26	1.05	0.83	125	0.27	1.64
5	252 ± 2	0.91	0.82	0.54	108	0.21	1.68
7	519 ± 1	1.49	0.22	0.3	419	0.001	3.42
10	283 ± 14	0.89		0.57	165	0.25	1.8
13	329 ± 29	1.22		0.85	103	0.2	2.08
79	252 ± 28	0.67		0.5	230	0.011	1.53

[a]Kinetic constant normalized by BET surface areas were calculated by using surface areas given in Table 1.
[b]k_{diss} kinetic constants were recalculated for situ-temperature assuming an activation energy of 60 kJ/mol by [Eq. (4)].
[c]Averaged of the dSi concentration in pore water at 0 - 2 cm. Note the situ-dSi concentration of station seven was sampled at the same site in June 2015.
[d]The situ-dSi dissolution rate was reconstructed from the situ-k_{diss} and situ-dSi concentrations using [Eq. (2)].

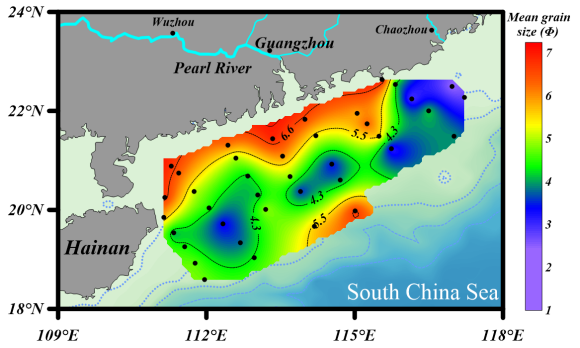

FIGURE 5
Distribution of $bSiO_2$/OC molar ratio in surface sediments of the NSCS.

part of organic matter, a great linear regression of TN versus OC in sediments with an intercept of zero demonstrates the two components are preserved in a well coupled manner, whether in finer or coarser sediments (Figure 7A). However, the positive linear relationship between OC (%) and $bSiO_2$ (%) has a higher slope (3.0) in fine-grained ($\Phi > \sim 5.5$) sediments than in coarser ($\Phi < \sim 5.5$) sediments (0.78) (Figure 7B), which suggests not only that fine-grained particles have better preservation performance for biogenic material, but also with each equal additional amount of OC stored, the fine-grained sediments will retain 2.8 times more $bSiO_2$ than coarser sediments in the NSCS. Furthermore, the average molar ratio of $bSiO_2$/OC in finer sediments (0.34 ± 0.07) (mainly at the inner shelf and upper slope) is lower than in coarser sediments (0.57 ± 0.17) (mainly at the outer shelf) (Figure 6). Therefore, there is a mismatch between the (diatom biomass)/(total phytoplankton biomass) ratio and the sedimentary $bSiO_2$/OC ratio in the inner shelf and outer shelf. The outer-shelf region with coarser sediments has been described as a sandy swath, and the sandy swath is the product of glacial sea level low stand and exposition to winnowing by strong bottom current recently (Wang and Li, 2009). The higher SiO_2/OC ratio, relative to the inner shelf and upper slope, could potentially be due to the higher energy level of this area. High-energy conditions could lead to more resuspension of sediments than low-energy environments and prompt longer oxygen exposure time, which in turn leads to lower OC contents through selective degradation of

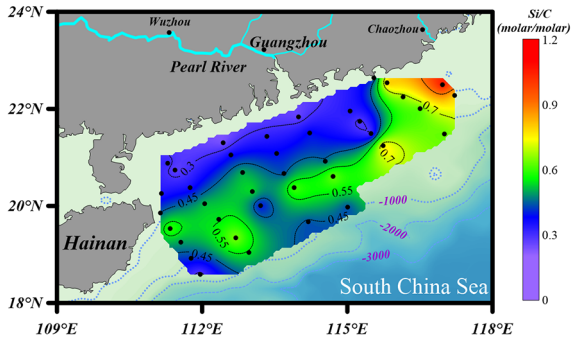

FIGURE 6
Distribution of mean grain size (Φ) in surface sediments of the NSCS.

labile young fractions and reduced TOC content (Van der Voort et al., 2018). Compared with the silicic acid degree of unsaturation, the demand of oxygen is much smaller for the dissolution of $bSiO_2$. The mismatch at the inner shelf is discussed in section 4.3.

4.2 The influence of aluminum and detrital material

The solubilities of $bSiO_2$ in the NSCS sediments (298 ± 94 μM) is seriously inhibited, which exhibits a low level compared with some marginal seas and open oceans (Figure 8). It has been proven that aluminum is probably the most significant factor affecting spatial variations in measured $bSiO_2$ solubility (Dixit et al., 2001). Field data and laboratory experiments reveal that the structural incorporation of Al into the silica framework by substituting Si atoms in the silica lattice reduces the solubility whether during the living diatom biomineralization process, settling after death, or deposited on the seafloor (Van Bennekom et al., 1991; Van Beueskom et al., 1997; Gehlen et al., 2002; Van Cappellen et al., 2002; Koning et al., 2007). The Pearl River delivers a high concentration of Al (360 – 690 nmol L^{-1}) to the NSCS and observes a shelf–to-slope transportation pattern (Zhang et al., 2020). Due to this severe terrigenous effect, the dissolved Al concentrations of seawater in the NSCS was reported to be at a high level (8 – 59 nmol L^{-1}, with an average of 30 ± 11 nmol L^{-1}) with a seaward decline (Guo, 2016), which is higher than some marginal seas, such as the Arabian Sea (3 – 15 nmol L^{-1}) and the Weddell-Scotia Seas (1 – 3 nmol L^{-1}) (Van Bennekom et al., 1991; Schüßler et al., 2005), and is much higher than some open oceans, such as the Pacific Ocean (0.3 – 5 nmol L^{-1}), the North Atlantic (6 – 25 nmol L^{-1}), and the Southern Ocean (0.33 – 0.8 nmol L^{-1}) (Orians and Bruland, 1986; Kramer et al., 2004; Middag et al., 2011). The scavenging proportion of the dissolved Al by phytoplankton was reported as up to 9.4 – 25.7% in summer (Zhang et al., 2020). Culture diatoms in Al-enriched solution exhibit a 20% lower solubility than in Al-depleted solution at 3 °C (Gallinari et al., 2002). The "primary uptake" of Al in the water column probably explains part of the reason why the solubility of the NSCS sediment is lower than some other sea areas. More important is the "Al – detrital – $bSiO_2$" interactions during early diagenesis of $bSiO_2$ in sediments. On one hand, the concentration of Al in pore water generally is several or tens of times (100 – 500 nmol L^{-1}) higher than seawater (Koning et al., 2007), which drives the "secondary uptake" of $bSiO_2$ debris. The well correlation between the dissolved Al concentration in pore water with the detrital/opal ratio in sediments confirms the detrital materials as an important source of Al (Dixit et al., 2001). The increase in Al levels often happens at the sediment-water interface (Van Cappellen and Qiu, 1997b). The high detrital matter content (80.9% ± 12.4%) in the NSCS sediments, which is higher than the Arabian Sea (30% – 50%), the Peru-Basin (66% ± 1%), and the Scotia Sea (36% - 66%) (Rickert, 2000), provides an abundance of Al to restrain the $bSiO_2$ dissolution and solubility. On the other hand, as the $bSiO_2$ deposited at the sediment-water interface, the continuously releasing Al (also including other ions, i.e., Mg^{2+}, K^+, and F^-) from detrital-rich sediments can induce

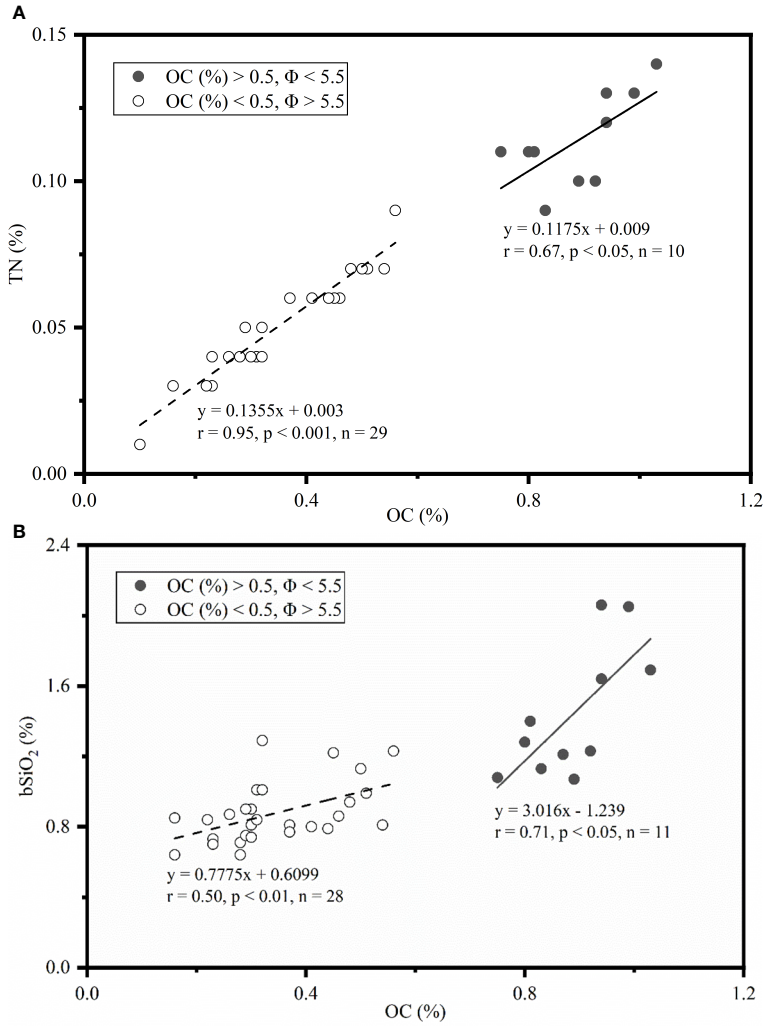

FIGURE 7
Correlations between **(A)** OC (%) and TN (%), and **(B)** OC (%) and $bSiO_2$ (%) contents in sediments with Pearson correlation coefficients (r) and regression curves. Solid and dashed lines denote the regression trends with OC > 0.5 and Φ< 5.5, and OC<0.5 and Φ > 5.5, respectively.

reprecipitation with dSi and $bSiO_2$ to form authigenic silicates or adsorb onto the surfaces of $bSiO_2$ to further reduce the solubility (Van Cappellen and Qiu, 1997b; Dixit et al., 2001; Michalopoulos and Aller, 2004; Loucaides et al., 2010), which is called reverse weathering. It has been proven a crucial pathway that can remove large amounts of silica from ocean within a short time (months to years) (Michalopoulos and Aller, 2004; Rahman et al., 2017; Tréguer et al., 2021). Rickert et al. (2002) used sediment samples pretreated with 10% HCl and H_2O_2 in the Scotia Sea and found that the solubility increased by 104% and the dissolution rate constant increased by 590% compared to unpretreated samples. The specific surface areas also increased by a factor of two to three times due to the pretreatment procedure (removing the organic coating and partially authigenic minerals). These results were attributed to the detrital minerals or authigenic aluminosilicates forming on the $bSiO_2$ surface, some of which could readily dissolve in mild HCl solution. Loucaides et al. (2010) reinforced the view by long-term incubation experiments (fresh diatom frustules were separated from the terrigenous sediments by a dialysis membrane, only allowing the exchange of dissolved species), and demonstrated the interaction between $bSiO_2$, seawater, and lithogenic minerals dramatically inhibits the solubility of $bSiO_2$ by forming new mineral precipitates on $bSiO_2$ surface. Our results showed that a strong correlation between solubility and detrital or detrital to $bSiO_2$ ratio (Figure 9). Gallinari et al. (2002) used different diatom species mixed with variable amounts of silicate minerals in a batch experiment, which presented a similar correlation between solubility and detrital to $bSiO_2$ ratios. This evidence supported our conclusion that the "Al – detrital – $bSiO_2$" interactions play important retarding roles in solubility space variation of $bSiO_2$ in the sediments of the NSCS.

4.3 The influence of specific surface area and particle size

Variations of specific surface area (SSA) must be considered when comparing the dissolution properties of sedimentary $bSiO_2$

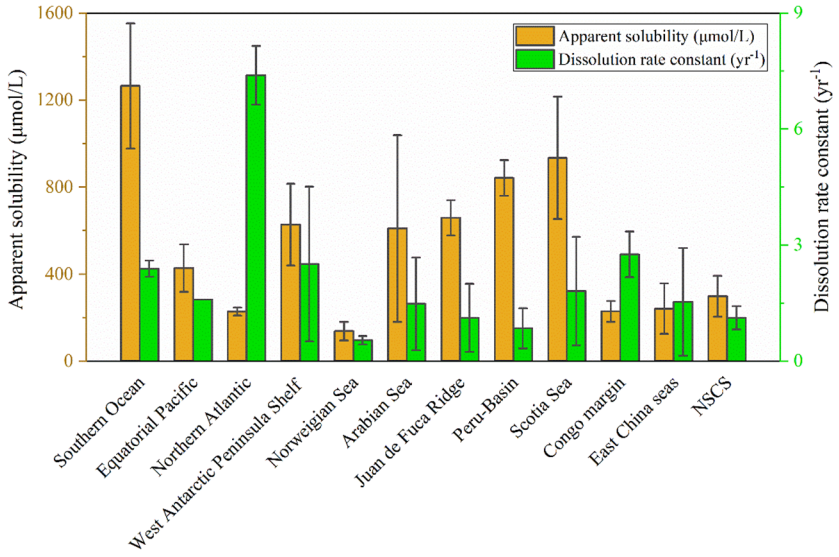

FIGURE 8
The solubilities and dissolution rate constants determined in this study for the NSCS sediments compared with other marginal seas or open oceans, including: the Southern Ocean (Van Cappellen and Qiu, 1997a; Van Cappellen and Qiu, 1997b), the Equatorial Pacific (Gallinari et al., 2002), the Northern Atlantic [averaged data from Gallinari et al. (2002); Gallinari et al. (2008) and Ragueneau et al. (2001)], the West Antarctic Peninsula Shelf (Gallinari et al., 2008), the Norweigian Sea (Rickert, 2000), the Arabian Sea (Rickert, 2000), the Juan de Fuca Ridge (Rickert, 2000), the Peru-Basin (Rickert, 2000), the Scotia Sea (Rickert, 2000), the Congo margin (Ragueneau et al., 2009), and east China seas (containing the Yellow Sea and the East China Sea) (Wu et al., 2017; Wu and Liu, 2020). Note that all the dissolution rate constants have been recalculated at 25°C using Eq. (4) for the purpose of comparison.

and siliceous plankton in marine surface waters (Van Cappellen et al., 2002). It is generally believed that the SSA can provide a reliable proxy to represent the availability of solid surface area for solution reaction (Hurd, 1973). The dissolution rate constant of freshly exposed diatom frustules measured in labs can be as high as ~16 yr^{-1}, and the SSA of diatom frustules varied from 16 to 260 m^2 g^{-1} (Van Cappellen et al., 2002), which are much higher than that in the NSCS sediments (~ 1.12 yr^{-1} and ~ 7.1 m^2 g^{-1}) (Table 1). In this regard, the lower rate constants and SSA values in sediments reflects that the preferential dissolution of the part with higher SSA in heterogeneous siliceous components, or the highly reactive part of $bSiO_2$ was regenerated during the settling process in the water column.

The reaction rate constants measured under the same conditions should reflect the relative differences of reactive surface areas (or reactive surface sites) (Rickert et al., 2002). However, it seems that sediment bulk SSA can be used as a proxy for the reactivity of $bSiO_2$ in the NSCS at some stations, such as station one and seven, which exhibit the highest dissolution rate constants corresponding to the highest SSA values. An abnormal phenomenon occurred at station four, which presented a relatively higher dissolution rate constant but very low SSA value. Our data overall presented a weak correlation between the dissolution rate constants and the sediment SSA, particle sizes, or $bSiO_2$ loadings (Tables 1, 2). Rickert et al. (2002) reported that the correlation of reaction rate constants and sediment SSA were only found in almost pure $bSiO_2$ samples (cultured phytoplankton or acid-cleaned samples from the water column), excluding pure siliceous oozes ($bSiO_2$ contents > 49%), whereas the adsorption capacity of the $bSiO_2$ for cobalt ions well corresponded to the reactivity changes (Van Cappellen and Qiu, 1997b). The BET surface area of siliceous ooze cores in the Southern Ocean basically remains unchanged with increasing depth, whereas the reaction rate constants still decrease by three times when the depth reaches 30 cm (Van Cappellen, 1996). However, elemental and microscopic analyses showed no changes in mineral composition or any diagenetic alterations throughout the sediment cores. This evidence implies that the reactivity of the $bSiO_2$ surface has altered but not the geometric surface area determined by nitrogen BET, which has been called a progressive "aging" process of the $bSiO_2$ surface (loss of reactive surface sites) (Van Cappellen, 1996). This "aging" process may be related to surface charge density (Dixit and Van Cappellen, 2002; Loucaides et al., 2010). It is worth noting that all of the FTIR (Fourier-transform infrared) spectroscopic evidence (Schmidt et al., 2001), the apparent reactivity rate constants obtained from leaching alkaline solution (Koning et al., 1997), and from flow-through experiment (Rickert et al., 2002) manifest that the loss of reactive surface sites has already begun as the $bSiO_2$ settles down in the water column. The sediment flux of the Pearl River is transported to the NSCS in the form of a plume, which presents distinct seasonal variations influenced by the East Asian monsoon: during summer, under the effect of weak southwest winds (~ 6 m s^{-1}), the water mass at the inner-shelf moves eastward, but the suspended particles of the Pearl River plume are still predominantly transported to the west due to the prevalent coastal current (Figure 1B); during winter, the coastal current is strengthened by the strong northeasterly winds (~ 9 m s^{-1}), which can resuspend sediments and keep them transporting westward (Figure 1C) (Liu et al., 2014). The dissolution rate constants of $bSiO_2$ on the east side of the Pearl River estuary (0.67 yr^{-1}, station 79) are distinctly lower than those

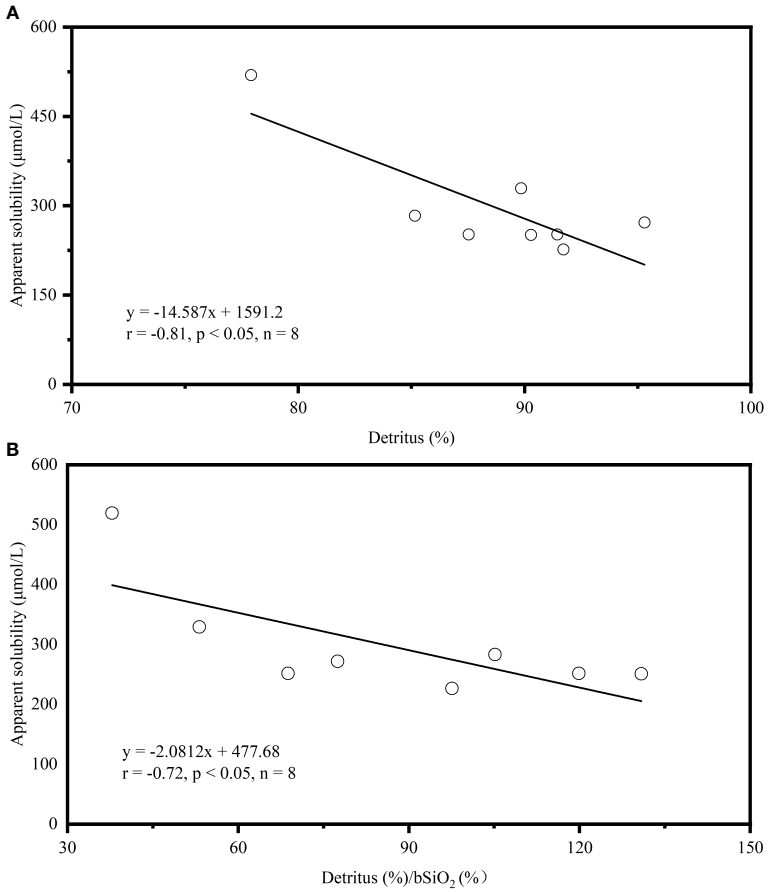

FIGURE 9
Correlations between **(A)** $bSiO_2$ apparent solubility (μmol/L) and detrital material content (%), and **(B)** $bSiO_2$ apparent solubility (μmol/L) and detrital material (%)/$bSiO_2$ (%) in sediments of the NSCS. The Pearson correlation coefficients (r) and regression curves are shown.

on the west side (1.22 yr^{-1}, station 13). Furthermore, the sedimentation rate on the west (~ 1cm yr^{-1}) side of the Pearl River estuary is much higher than on the east side (~ 0.5 cm yr^{-1}). We suggest that resuspension-deposition and higher sedimentation rate maintain the fresh $bSiO_2$ in the surface sediment on the west side of the Pearl River estuary and result in the high reactive of $bSiO_2$ in the surface sediments. It is completely different for the degradation of OC. Wei et al. (2020) reported older terrigenous OC on the west (1950 yr BP) side of the Pearl River estuary than on the east (1510 yr BP) due to resuspension-deposition. Repeated resuspension-deposition cycles could promote oxygen exposure time and accelerate the remineralization of fresh OC, and leave the refractory older OC, whereas redox oscillations have little impact on the dissolution of $bSiO_2$. This is probably also the reason why the highest (diatom biomass)/(total phytoplankton biomass) ratio in surface water but the lowest $bSiO_2$/OC ratio was recorded in the sediments of the west inner-shelf region (Figure 6). Besides the "aging" process, the vertical transport of $bSiO_2$ through the fast settling of aggregates or fecal pellets also play a role (Shi et al., 2019), trying to maintain the initial reactivity of $bSiO_2$ of the surface ocean, such as at station one with lower water depth and higher reactivity. In this case, the most important parameter could be the degree of coupling between surface waters and the seabed. For example, the formation of blooms and the rapid sedimentation of diatoms, either in the form of large aggregates or embedded within fecal pellets of large euphausiids (Nelson et al., 1995), could lead to the deposition of fresh diatoms with dissolution properties similar to those encountered in surface waters. Our sediment samples are located in a wide range of water depths (40 – 773 m), and subjected to intense turbulence by active water dynamics or sediment resuspension due to the buoyancy of river plumes, wind force, or terrigenous impact (Cao et al., 2020). The partly unsatisfactory agent of SSA for the reactivity surface of our samples presumably reflected the different "aging" or other water column processes (i.e., forming diatom aggregation or fecal pellets) of $bSiO_2$ particles when sinking in the water column.

4.4 Implications for the preservation of $bSiO_2$ in the NSCS sediments

The dissolution of $bSiO_2$ is very sensitive to temperature changes, and preservation status largely depends on the difference of *in situ* temperature (Kamatani and Riley, 1979; Van Cappellen and Qiu, 1997b). To further discuss the *in situ* preservation mechanism of $bSiO_2$ in the NSCS sediments, the measured

reaction rates were reconstructed under *in situ* conditions. We applied an average activation energy (E_{app}) of 60 kJ/mol to obtain the rate constants at *in situ* temperature using the equation (Rickert et al., 2002):

$$lnk_2 = lnk_1 + \frac{E_{app}}{R}\left[\frac{1}{T_1} - \frac{1}{T_2}\right] \quad (4)$$

where R = 8.314 J K^{-1} mol^{-1} and T (K) donates the temperature, k refers to the rate constant (yr^{-1}). The pressure was not considered because it has little influence within water depths of 800 m (Loucaides et al., 2012). The dissolution rate constants of $bSiO_2$ in the NSCS sediments at *in situ* temperature were 0.94 ± 0.13 yr^{-1}, 0.61 ± 0.13 yr^{-1}, and 0.30 yr^{-1} at the inner shelf, outer shelf, and upper slope, respectively (Table 2). The upper depth (2 cm) interval corresponds to the zone of net silica dissolution. Then, the net dissolution rate of $bSiO_2$ at the eight stations of the 2 cm surface sediments were reconstruct by combining the experimental derived non-linear dissolution law (Eq. (2), Figure 10) with the *in situ* pore water dSi concentration (averaged of 0 - 2 cm), which were 0.20 ± 0.01 yr^{-1}, 0.18 ± 0.11 yr^{-1}, and 0.001 yr^{-1} at the inner shelf, outer shelf, and upper slope, respectively (Table 2). The reconstructed *in situ* dissolution rate in the upper slope (station seven) is orders lower than that at the shelf. This suggests that the differences of $bSiO_2$ preservation between the inner shelf, outer shelf, and upper slope were the results of a wide range of *in situ* temperature-induced differences of dissolution rates constants and the departure from equilibrium-induced differences of *in situ* dissolution rates. These results showed dissolution kinetics-controlled evidence that explains the mismatch between the (diatom biomass)/(total phytoplankton biomass) ratio and the sedimentary $bSiO_2$/OC ratio in the inner shelf and outer shelf, and also a mismatch between the $bSiO_2$ primary productivity and the $bSiO_2$ sediment records in the upper slope of the NSCS. The mismatch of $bSiO_2$/OC ratio at the outer shelf is due to high-energy conditions and the mismatch at the inner shelf is attributed to the resuspension-deposition, which have been discussed in section 4.1 and section 4.3. The high reconstructed *in situ* rate constants (0.94 ± 0.13 yr^{-1}) and dissolution rate (0.20 ± 0.01 yr^{-1}) strengthened the fact of the lower $bSiO_2$/OC ratio observed at the inner shelf. Wei et al. (2020) suggested that surface sediments at the slope displayed a relatively higher terrigenous OC content and older terrigenous OC than that at the outer shelf, likely due to cross-shelf transport from the Pearl River and sediment winnowing on the outer shelf. Our results suggest that the lower *in situ* reactivity (0.30 yr^{-1}) and dissolution rate (0.001 yr^{-1}) allowed sedimentary $bSiO_2$ to be well preserved in this area.

The degree of undersaturation of the pore fluid represents the thermodynamic driving force for the dissolution process and is directly dependent on the solubility of the $bSiO_2$ (Van Cappellen and Qiu, 1997a). The dissolution rates were plotted against the departure from saturation state (Figure 10), which exhibits a non-linear dissolution kinetic, which was also observed in different deposition settings (Van Cappellen and Qiu, 1997a; Van Cappellen and Qiu, 1997b; Rickert et al., 2002; Ragueneau et al., 2009). The non-linear dissolution kinetics implied a higher dissolution rate in a highly unsaturated silicic solution, that is, more efficient recycling of $bSiO_2$ in dSi-depleted upper sediments compared with deep sediments, which is meaningful for benthic Si regeneration. However, the non-linear dissolution kinetics must be severely inhibited by the high contents of detritus in the NSCS sediments. The overall dissolution rate constants of $bSiO_2$ in the NSCS sediments was 1.12 ± 0.3 yr^{-1} at 25°C, which is lower than some marginal seas, such as the West Antarctic Peninsula Shelf [2.5 yr^{-1}, Gallinari et al. (2008)], the Arabian Sea [1.48 ± 1.4 yr^{-1}, Rickert (2000)], the Scotia Sea [1.81 ±

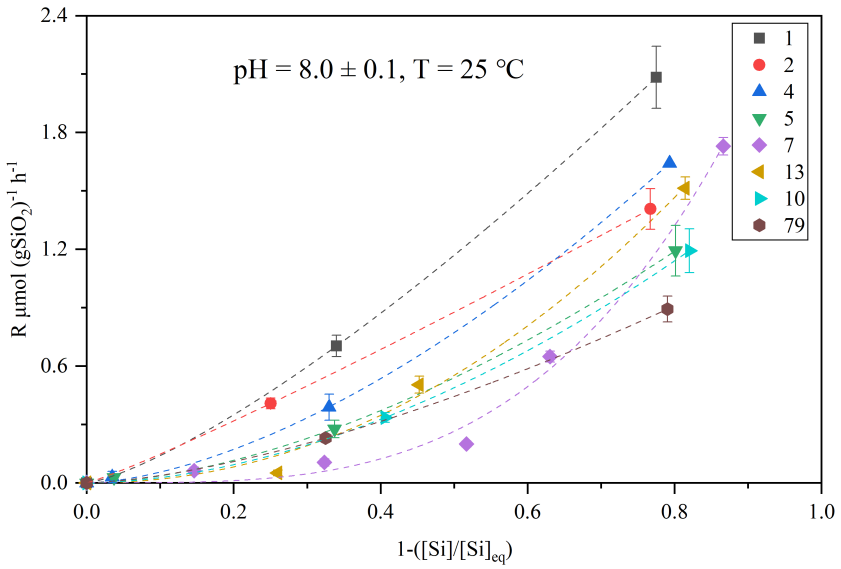

FIGURE 10
Experimental dissolution rates [μmol $(gSiO_2)^{-1}$ h^{-1}] plotted versus the departure from equilibrium. The dashed line is the curve fitted by the experimental data using Eq. (2). The legends ansssd numbers in the upper right corner indicate different stations conducted flow-through experiments. The uncertainties are shown by error bars.

1.4 yr^{-1}, Rickert (2000)], and the east China seas (containing the Yellow Sea and the East China Sea, 1.53 ± 1.39 yr^{-1} [Wu et al. (2017); Wu and Liu (2020)]; it is also lower than some open oceans, such as the Southern Ocean [2.39 ± 0.2 yr^{-1}, Van Cappellen and Qiu (1997b)], the equatorial Pacific [1.59 yr^{-1}, Gallinari et al. (2002)], and especially the North Atlantic [7.39 yr^{-1}, Ragueneau et al. (2001)] (Figure 8). The extremely high reaction rate constants of the $bSiO_2$ in sediments or the sediment trap of the North Atlantic Ocean are believed to be an important reason for the very low $bSiO_2$ contents (~1%) and poor preservation efficiency (12%) in the sediments compared with the Southern Ocean (Rickert, 2000; Ragueneau et al., 2001). Inversely, the relatively low reaction rate constants in the NSCS may be responsible for the well preservation efficiency of the $bSiO_2$ (27%) (Ma et al., 2022). Therefore, our results support the view that continental margin sediments play significant roles as silica sinks in the marine silica budget (DeMaster, 2002).

5 Conclusion

The $bSiO_2$ content in surface sediments of the NSCS ranged from 0.64% to 2.06%, with an average of 1.04% ± 0.35%. A strong zonal distribution tendency of the $bSiO_2$ distribution was observed, decreasing first and then increasing from the inner shelf to the upper slope. The excellent coupling accumulation of $bSiO_2$ and OC exhibits different preservation patterns in finer and coarser sediments compared with TN and OC. The solubility and dissolution kinetics in the NSCS sediments were at a relative low level (solubility: 298 ± 94 μM; dissolution rate constant: 1.12 ± 0.3 yr^{-1}) compared with other marginal seas and open oceans, likely due to the high Al concentration in the water column and the high content of lithogenic material in sediments. In addition, the distribution of satellite remote-sensed Chl-a, the proportion of diatoms in total biomass of phytoplankton, and the variation of surface primary productivity all point to a mismatch between the (diatom biomass)/(total phytoplankton biomass) ratio and the sedimentary $bSiO_2$/OC ratio at the inner shelf and outer shelf, and also a mismatch between the $bSiO_2$ primary productivity and the $bSiO_2$ sediment records at the upper slope of the NSCS. The resuspension-deposition and the higher reconstructed *in situ* rate constants (0.94 ± 0.13 yr^{-1}) and dissolution rate (0.20 ± 0.01 yr^{-1}) were responsible for the lower $bSiO_2$/OC ratio (0.45 ± 0.28) at the inner shelf, and the winnowing process at the outer shelf with a lower reconstructed *in situ* reactivity (0.30 yr^{-1}) and dissolution rate (0.001 yr^{-1}) led to the good preservation of $bSiO_2$ at the upper slope. The NSCS sediments may serve as an important silica sink in the global silicon cycle due to lower reactivity in comparison with other ocean areas.

Data availability statement

The raw data supporting the conclusions of this article will be made available by the authors, without undue reservation.

Author contributions

YM: conception and design of study. SML: financial support. YM: drafting the manuscript. SML, DZ and WL: revising the manuscript. YM, BY, NZ, and JH: acquisition of data. YM: interpretation of data. All authors contributed to the article and approved the submitted version.

Funding

This study was funded by the Natural Sciences Foundation of China (NSFC: 41376086), the Taishan Scholars Programme of Shandong Province, Aoshan Talents Program supported by the Qingdao National Laboratory for Marine Science and Technology (No. 2015ASTP-OS08). This study is a contribution to the IMBeR Program.

Acknowledgments

We thank the captain and crews of the R/V “Shi Yan 3” for their help during the sampling expeditions.

Conflict of interest

The authors declare that the research was conducted in the absence of any commercial or financial relationships that could be construed as a potential conflict of interest.

Publisher’s note

References

Bidle, K. D., and Azam, F. (1999). Accelerated dissolution of diatom silica by marine bacterial assemblages. *Nature* 397 (6719), 508–512. doi: 10.1038/17351

Bidle, K. D., and Azam, F. (2001). Bacterial control of silicon regeneration from diatom detritus: significance of bacterial ectohydrolases and species identity. *Limnology Oceanography* 46 (7), 1606–1623. doi: 10.4319/lo.2001.46.7.1606

Bidle, K. D., Brzezinski, M. A., Long, R. A., Jones, J. L., and Azam, F. (2003). Diminished efficiency in the oceanic silica pump caused by bacteria-mediated silica dissolution. *Limnology Oceanography* 48 (5), 1855–1868. doi: 10.4319/lo.2003.48.5.1855

Brzezinski, M. A., and Nelson, D. M. (1989). Seasonal changes in the silicon cycle within a gulf stream warm-core ring. *Deep Sea Res. Part A. Oceanographic Res. Papers* 36 (7), 1009–1030. doi: 10.1016/0198-0149(89)90075-7

Brzezinski, M. A., and Nelson, D. M. (1995). The annual silica cycle in the Sargasso Sea near Bermuda. *Deep Sea Res. Part I: Oceanographic Res. Papers* 42 (7), 1215–1237. doi: 10.1016/0967-0637(95)93592-3

Cai, P., Zhao, D., Wang, L., Huang, B., and Dai, M. (2015). Role of particle stock and phytoplankton community structure in regulating particulate organic carbon export in a large marginal sea. *J. Geophysical Research: Oceans* 120 (3), 2063–2095. doi: 10.1002/2014JC010432

Cao, Z., Wang, D., Zhang, Z., Zhou, K., Liu, X., Wang, L., et al. (2020). Seasonal dynamics and export of biogenic silica in the upper water column of a large marginal sea, the northern south China Sea. *Prog. Oceanography* 188, 102421. doi: 10.1016/j.pocean.2020.102421

Chen, Y.-L. L. (2005). Spatial and seasonal variations of nitrate-based new production and primary production in the south China Sea. *Deep Sea Res. Part I: Oceanographic Res. Papers* 52 (2), 319–340. doi: 10.1016/j.dsr.2004.11.001

Chen, C.-C., Shiah, F.-K., Chung, S.-W., and Liu, K.-K. (2006). Winter phytoplankton blooms in the shallow mixed layer of the south China Sea enhanced by upwelling. *J. Mar. Syst.* 59 (1-2), 97–110. doi: 10.1016/j.jmarsys.2005.09.002

Cheng, T., Hammond, D. E., Berelson, W. M., Hering, J. G., and Dixit, S. (2009). Dissolution kinetics of biogenic silica collected from the water column and sediments of three southern California borderland basins. *Mar. Chem.* 113 (1-2), 41–49. doi: 10.1016/j.marchem.2008.12.001

DeMaster, D. J. (1981). The supply and accumulation of silica in the marine environment. *Geochim. Cosmochim. Acta* 45 (10), 1715–1732. doi: 10.1016/0016-7037(81)90006-5

DeMaster, D. J. (2002). The accumulation and cycling of biogenic silica in the southern ocean: revisiting the marine silica budget. *Deep Sea Res. Part II: Topical Stud. Oceanography* 49 (16), 3155–3167. doi: 10.1016/S0967-0645(02)00076-0

DeMaster, D. J., Knapp, G. B., and Nittrouer, C. A. (1983). Biological uptake and accumulation of silica on the Amazon continental shelf. *Geochimica Cosmochimica Acta* 47 (10), 1713–1723. doi: 10.1016/0016-7037(83)90021-2

DeMaster, D. J., Ragueneau, O., and Nittrouer, C. A. (1996). Preservation efficiencies and accumulation rates for biogenic silica and organic c, n, and p in high-latitude sediments: The Ross Sea. *J. Geophysical Research: Oceans* 101 (C8), 18501–18518. doi: 10.1029/96JC01634

Dixit, S., and Van Cappellen, P. (2002). Surface chemistry and reactivity of biogenic silica. *Geochimica Cosmochimica Acta* 66 (14), 2559–2568. doi: 10.1016/S0016-7037(02)00854-2

Dixit, S., Van Cappellen, P., and Van Bennekom, A. J. (2001). Processes controlling solubility of biogenic silica and pore water build-up of silicic acid in marine sediments. *Mar. Chem.* 73 (3-4), 333–352. doi: 10.1016/S0304-4203(00)00118-3

Dugdale, R. C., Wilkerson, F. P., and Minas, H. J. (1995). The role of a silicate pump in driving new production. *Deep Sea Res. Part I: Oceanographic Res. Papers* 42 (5), 697–719. doi: 10.1016/0967-0637(95)00015-X

Fraysse, F., Pokrovsky, O. S., Schott, J., and Meunier, J.-D. (2006). Surface properties, solubility and dissolution kinetics of bamboo phytoliths. *Geochimica Cosmochimica Acta* 70 (8), 1939–1951. doi: 10.1016/j.gca.2005.12.025

Gallinari, M., Ragueneau, O., Corrin, L., DeMaster, D. J., and Tréguer, P. (2002). The importance of water column processes on the dissolution properties of biogenic silica in deep-sea sediments i. solubility. *Geochimica Cosmochimica Acta* 66 (15), 2701–2717. doi: 10.1016/S0016-7037(02)00874-8

Gallinari, M., Ragueneau, O., DeMaster, D., Hartnett, H., Rickert, D., and Thomas, C. (2008). Influence of seasonal phytodetritus deposition on biogenic silica dissolution in marine sediments–potential effects on preservation. *Deep Sea Res. Part II: Topical Stud. Oceanography* 55 (22-23), 2451–2464. doi: 10.1016/j.dsr2.2008.06.005

Ge, Q., Liu, J. P., Xue, Z., and Chu, F. (2014). Dispersal of the zhujiang river (Pearl river) derived sediment in the Holocene. *Acta Oceanologica Sinica.* 33, 1–9. doi: 10.1007/s13131-014-0407-8

Gehlen, M., Beck, L., Calas, G., Flank, A.-M., Van Bennekom, A. J., and Van Beusekom, J. E. E. (2002). Unraveling the atomic structure of biogenic silica: evidence of the structural association of Al and Si in diatom frustules. *Geochimica Cosmochimica Acta* 66 (9), 1601–1609. doi: 10.1016/S0016-7037(01)00877-8

Guo, Y. (2016). Distribution of dissolved aluminum in the northern south China Sea and its influence factors. (Qingdao: Ocean University of China). (in Chinese with English abstract)

Han, A., Dai, M., Kao, S.-J., Gan, J., Li, Q., Wang, L., et al. (2012). Nutrient dynamics and biological consumption in a large continental shelf system under the influence of both a river plume and coastal upwelling. *Limnology Oceanography* 57 (2), 486–502. doi: 10.4319/lo.2012.57.2.0486

Ho, T.-Y., Chou, W.-C., Wei, C.-L., Lin, F.-J., Wong, G. T., and Line, H.-L. (2010). Trace metal cycling in the surface water of the south China Sea: vertical fluxes, composition, and sources. *Limnology Oceanography* 55 (5), 1807–1820. doi: 10.4319/lo.2010.55.5.1807

Hung, J.-J., Wang, S.-M., and Chen, Y.-L. (2007). Biogeochemical controls on distributions and fluxes of dissolved and particulate organic carbon in the northern south China Sea. *Deep Sea Res. Part II: Topical Stud. Oceanography* 54 (14-15), 1486–1503. doi: 10.1016/j.dsr2.2007.05.006

Hurd, D. C. (1973). Interactions of biogenic opal, sediment and seawater in the central equatorial pacific. *Geochimica Cosmochimica Acta* 37 (10), 2257–2282. doi: 10.1016/0016-7037(73)90103-8

Kamatani, A., Ejiri, N., and Treguer, P. (1988). The dissolution kinetics of diatom ooze from the Antarctic area. *Deep Sea Res. Part A. Oceanographic Res. Papers* 35 (7), 1195–1203. doi: 10.1016/0198-0149(88)90010-6

Kamatani, A., and Riley, J. P. (1979). Rate of dissolution of diatom silica walls in seawater. *Mar. Biol.* 55 (1), 29–35. doi: 10.1007/BF00391714

Khalil, K., Rabouille, C., Gallinari, M., Soetaert, K., DeMaster, D., and Ragueneau, O. (2007). Constraining biogenic silica dissolution in marine sediments: a comparison between diagenetic models and experimental dissolution rates. *Mar. Chem.* 106 (1-2), 223–238. doi: 10.1016/j.marchem.2006.12.004

Koning, E., Brummer, G. J., Van Raaphorst, W., Van Bennekom, J., Helder, W., and Van Iperen, J. (1997). Settling, dissolution and burial of biogenic silica in the sediments off Somalia (northwestern Indian ocean). *Deep-Sea Res. Part Ii-Topical Stud. Oceanography* 44 (6-7), 1341–1360. doi: 10.1016/S0967-0645(97)00018-0

Koning, E., Gehlen, M., Flank, A.-M., Calas, G., and Epping, E. (2007). Rapid post-mortem incorporation of aluminum in diatom frustules: Evidence from chemical and structural analyses. *Mar. Chem.* 106 (1-2), 208–222. doi: 10.1016/j.marchem.2006.06.009

Kramer, J., Laan, P., Sarthou, G., Timmermans, K., and De Baar, H. (2004). Distribution of dissolved aluminium in the high atmospheric input region of the subtropical waters of the north Atlantic ocean. *Mar. Chem.* 88 (3-4), 85–101. doi: 10.1016/j.marchem.2004.03.009

Krause, J. W., Nelson, D. M., and Brzezinski, M. A. (2011). Biogenic silica production and the diatom contribution to primary production and nitrate uptake in the eastern equatorial pacific ocean. *Deep-Sea Res. Part Ii-Topical Stud. Oceanography* 58 (3-4), 434–448. doi: 10.1016/j.dsr2.2010.08.010

Krumbein, W. C. (1934). Size frequency distributions of sediments. *J. Sedimentary Res.* 4 (2), 65–77. doi: 10.1306/D4268EB9-2B26-11D7-8648000102C1865D

Lawson, D. S., Hurd, D. C., and Pankratz, H. S. (1978). Silica dissolution rates of decomposing phytoplankton assemblages at various temperatures. *Am. J. Sci.* 278 (10), 1373–1393. doi: 10.2475/ajs.278.10.1373

Liu, Y., Dai, M., Chen, W., and Cao, Z. (2012). "Distribution of biogenic silica in the upwelling zones in the south China Sea," in *Advances in geosciences*, vol. 28. (Atmospheric Science (AS) & Ocean Science (OS), 55–65.

Liu, S. M., De Zhu, B., Zhang, J., Wu, Y., Liu, G. S., Deng, B., et al. (2010). Environmental change in jiaozhou bay recorded by nutrient components in sediments. *Mar. pollut. Bull.* 60 (9), 1591–1599. doi: 10.1016/j.marpolbul.2010.04.003

Liu, Y., Gao, S., Wang, Y. P., Yang, Y., Long, J., Zhang, Y., et al. (2014). Distal mud deposits associated with the pearl river over the northwestern continental shelf of the south China Sea. *Mar. Geology.* 347, 43–57. doi: 10.1016/j.margeo.2013.10.012

Liu, S., Hong, G.-H., Zhang, J., Ye, X., and Jiang, X. (2009). Nutrient budgets for large Chinese estuaries. *Biogeosciences* 6 (10), 2245–2263. doi: 10.5194/bg-6-2245-2009

Liu, S., Ye, X., Zhang, J., and Zhao, Y. (2002). Problems with biogenic silica measurement in marginal seas. *Mar. Geology* 192 (4), 383–392. doi: 10.1016/S0025-3227(02)00531-5

Liu, Z., Zhao, Y., Colin, C., Stattegger, K., Wiesner, M. G., Huh, C.-A., et al. (2016). Source-to-sink transport processes of fluvial sediments in the south China Sea. *Earth-Science Rev.* 153, 238–273. doi: 10.1016/j.earscirev.2015.08.005

Loucaides, S., Behrends, T., and Van Cappellen, P. (2010). Reactivity of biogenic silica: Surface versus bulk charge density. *Geochimica Cosmochimica Acta* 74 (2), 517–530. doi: 10.1016/j.gca.2009.10.038

Loucaides, S., Koning, E., and Van Cappellen, P. (2012). Effect of pressure on silica solubility of diatom frustules in the oceans: Results from long-term laboratory and field incubations. *Mar. Chem.* 136, 1–6. doi: 10.1016/j.marchem.2012.04.003

Loucaides, S., Van Cappelle, P., and Behrends, T. (2008). Dissolution of biogenic silica from land to ocean: Role of salinity and pH. *LimOc* 53 (4), 1614–1621. doi: 10.4319/lo.2008.53.4.161

Ma, Y., Zhang, L., Liu, S., and Zhu, D. (2022). Silicon balance in the south China Sea. *Biogeochemistry*, 157, 327–353. doi: 10.1007/s10533-021-00879-4

Michalopoulos, P., and Aller, R. C. (2004). Early diagenesis of biogenic silica in the Amazon delta: Alteration, authigenic clay formation, and storage. *Geochimica Cosmochimica Acta* 68 (5), 1061–1085. doi: 10.1016/j.gca.2003.07.018

Middag, R., Van Slooten, C., De Baar, H., and Laan, P. (2011). Dissolved aluminium in the southern ocean. *Deep Sea Res. Part II: Topical Stud. Oceanography* 58 (25-26), 2647–2660. doi: 10.1016/j.dsr2.2011.03.001

Moriceau, B., Garvey, M., Ragueneau, O., and Passow, U. (2007). Evidence for reduced biogenic silica dissolution rates in diatom aggregates. *Mar. Ecol. Prog. Ser.* 333, 129–142. doi: 10.3354/meps333129

Mortlock, R., Charles, C., Froelich, P., Zibello, M., Saltzman, J., Hays, J., et al. (1991). Evidence for lower productivity in the Antarctic ocean during the last glaciation. *Nature* 351 (6323), 220–223. doi: 10.1038/351220a0

Mortlock, R. A., and Froelich, P. N. (1989). A simple method for the rapid determination of biogenic opal in pelagic marine sediments. *Deep Sea Res. Part A Oceanographic Res. Papers* 36 (9), 1415–1426. doi: 10.1016/0198-0149(89)90092-7

Müller, G. (1966). Grain size, carbonate content, and carbonate mineralogy of recent sediments of the Indian ocean off the eastern coast of Somalia. *Naturwissenschaften* 53 (21), 547–550. doi: 10.1007/BF00602953

Nelson, D. M., DeMaster, D. J., Dunbar, R. B., and Smith, W. O.Jr. (1996). Cycling of organic carbon and biogenic silica in the southern ocean: Estimates of water-column

and sedimentary fluxes on the Ross Sea continental shelf. *J. Geophysical Research: Oceans* 101 (C8), 18519–18532. doi: 10.1029/96JC01573

Nelson, D. M., and Dortch, Q. (1996). Silicic acid depletion and silicon limitation in the plume of the Mississippi river: evidence from kinetic studies in spring and summer. *Mar. Ecol. Prog. Ser.* 136, 163–178. doi: 10.3354/meps136163

Nelson, D. M., Tréguer, P., Brzezinski, M. A., Leynaert, A., and Quéguiner, B. (1995). Production and dissolution of biogenic silica in the ocean: Revised global estimates, comparison with regional data and relationship to biogenic sedimentation. *Global Biogeochemical Cycles* 9 (3), 359–372. doi: 10.1029/95GB01070

Ning, X. R., Chai, F., Xue, H., Cai, Y., Liu, C., and Shi, J. (2004). Physical-biological oceanographic coupling influencing phytoplankton and primary production in the South China Sea. *J. Geophys. Res.* 109, C10005. doi: 10.1029/2004JC002365

Orians, K. J., and Bruland, K. W. (1986). The biogeochemistry of aluminum in the pacific ocean. *Earth Planetary Sci. Lett.* 78 (4), 397–410. doi: 10.1016/0012-821X(86)90006-3

Pan, X., Wong, G. T., Tai, J.-H., and Ho, T. Y. (2015). Climatology of physical hydrographic and biological characteristics of the Northern South China Sea Shelf-sea (NoSoCS) and adjacent waters: Observations from satellite remote sensing. *Deep Sea Research Part II: Topical Studies in Oceanography* 117, 10–22. doi: 10.1016/j.dsr2.2015.02.022

Ragueneau, O., Gallinari, M., Corrin, L., Grandel, S., Hall, P., Hauvespre, A., et al. (2001). The benthic silica cycle in the northeast Atlantic: annual mass balance, seasonality, and importance of non-steady-state processes for the early diagenesis of biogenic opal in deep-sea sediments. *Prog. Oceanography* 50 (1-4), 171–200. doi: 10.1016/S0079-6611(01)00053-2

Ragueneau, O., Regaudie-de-Gioux, A., Moriceau, B., Gallinari, M., Vangriesheim, A., Baurand, F., et al. (2009). A benthic Si mass balance on the Congo margin: Origin of the 4000m DSi anomaly and implications for the transfer of Si from land to ocean. *Deep Sea Res. Part II: Topical Stud. Oceanography* 56 (23), 2197–2207. doi: 10.1016/j.dsr2.2009.04.003

Ragueneau, O., Schultes, S., Bidle, K., Claquin, P., and Moriceau, B. (2006). Si and C interactions in the world ocean: Importance of ecological processes and implications for the role of diatoms in the biological pump. *Global Biogeochemical Cycles* 20 (4), GB4502. doi: 10.1029/2006GB002688

Ragueneau, O., Tréguer, P., Leynaert, A., Anderson, R. F., Brzezinski, M. A., DeMaster, D. J., et al. (2000). A review of the Si cycle in the modern ocean: recent progress and missing gaps in the application of biogenic opal as a paleoproductivity proxy. *Global Planetary Change* 26 (4), 317–365. doi: 10.1016/S0921-8181(00)00052-7

Rahman, S., Aller, R. C., and Cochran, J. K. (2017). The missing silica sink: Revisiting the marine sedimentary Si cycle using cosmogenic 32Si. *Global Biogeochemical Cycles* 31 (10), 1559–1578. doi: 10.1002/2017GB005746

Rickert, D. (2000). Dissolution kinetics of biogenic silica in marine environments (German: Alfred Wegener Institute for Polar and Marine Research).

Rickert, D., Schlüter, M., and Wallmann, K. (2002). Dissolution kinetics of biogenic silica from the water column to the sediments. *Geochimica Cosmochimica Acta* 66 (3), 439–455. doi: 10.1016/S0016-7037(01)00757-8

Sayles, F., Martin, W., Chase, Z., and Anderson, R. (2001). Benthic remineralization and burial of biogenic SiO2, CaCO3, organic carbon, and detrital material in the southern ocean along a transect at 170 West. *Deep Sea Res. Part II: Topical Stud. Oceanography* 48 (19-20), 4323–4383. doi: 10.1016/S0967-0645(01)00091-1

Schmidt, M., Botz, R., Rickert, D., Bohrmann, G., Hall, S., and Mann, S. (2001). Oxygen isotopes of marine diatoms and relations to opal-a maturation. *Geochimica Cosmochimica Acta* 65 (2), 201–211. doi: 10.1016/S0016-7037(00)00534-2

Schrader, H., and Sorknes, R. (1991). Peruvian Coastal upwelling: Late quaternary productivity changes revealed by diatoms. *Mar. Geology* 97 (3-4), 233–249. doi: 10.1016/0025-3227(91)90118-N

Schüßler, U., Balzer, W., and Deeken, A. (2005). Dissolved Al distribution, particulate Al fluxes and coupling to atmospheric Al and dust deposition in the Arabian Sea. *Deep Sea Res. Part II: Topical Stud. Oceanography* 52 (14-15), 1862–1878. doi: 10.1016/j.dsr2.2005.06.005

Shi, Z., Liu, K., Zhang, S., Xu, H., and Liu, H. (2019). Spatial distributions of mesozooplankton biomass, community composition and grazing impact in association with hypoxia in the pearl river estuary. *Estuarine Coast. Shelf Sci.* 225, 106237. doi: 10.1016/j.ecss.2019.05.019

Tréguer, P., Sutton, J. N., Brzezinski, M., Charette, M. A., Devries, T., Dutkiewicz, S., et al. (2021). Reviews and syntheses: The biogeochemical cycle of silicon in the modern ocean. *Biogeosciences* 18, 1269–1289. doi: 10.5194/bg-18-1269-2021

Van Bennekom, A. J., Buma, A. G. J., and Nolting, R. F. (1991). Dissolved aluminium in the weddell-Scotia confluence and effect of Al on the dissolution kinetics of biogenic silica. *Mar. Chem.* 35 (1-4), 423–434. doi: 10.1016/S0304-4203(09)90034-2

Van Beueskom, J., Van Bennekom, A., Tréguer, P., and Morvan, J. (1997). Aluminium and silicic acid in water and sediments of the enderby and crozet basins. *Deep Sea Res. Part II: Topical Stud. Oceanography* 44 (5), 987–1003. doi: 10.1016/S0967-0645(96)00105-1

Van Cappellen, P. (1996). Reactive surface area control of the dissolution kinetics of biogenic silica in deep-sea sediments. *Chem. Geology* 132 (1-4), 125–130. doi: 10.1016/S0009-2541(96)00047-2

Van Cappellen, P., Dixit, S., and van Beusekom, J. (2002). Biogenic silica dissolution in the oceans: Reconciling experimental and field-based dissolution rates. *Global Biogeochemical Cycles* 16 (4), 23–21-23-10. doi: 10.1029/2001GB001431

Van Cappellen, P., and Qiu, L. (1997a). Biogenic silica dissolution in sediments of the southern ocean. i. solubility. *Deep Sea Res. Part II Topical Stud. Oceanography* 44 (5), 1109–1128. doi: 10.1016/S0967-0645(96)00113-0

Van Cappellen, P., and Qiu, L. (1997b). Biogenic silica dissolution in sediments of the southern ocean. II. kinetics. *Deep Sea Res. Part II: Topical Stud. Oceanography* 44 (5), 1129–1149. doi: 10.1016/S0967-0645(96)00112-9

Van der Voort, T. S., Mannu, U., Blattmann, T. M., Bao, R., Zhao, M., and Eglinton, T. I. (2018). Deconvolving the fate of carbon in coastal sediments. *Geophysical Res. Lett.* 45, 4134–4142. doi: 10.1029/2018GL077009

Wang, P., and Li, Q. (2009). *The south China Sea: Paleoceanography and sedimentology* (Netherlands: Springer), 506.

Ward, J., Hendry, K., Arndt, S., Faust, J. C., Freitas, F. S., Henley, S. F., et al. (2021). Stable silicon isotopes uncover a mineralogical control on the benthic silicon cycle in the Arctic barents Sea. *Geochimica et Cosmochimica Acta* 329, 206–230. doi: 10.1016/j.gca.2022.05.005

Wei, B., Mollenhauer, G., Hefter, J., Grotheer, H., and Jia, G. (2020). Dispersal and aging of terrigenous organic matter in the pearl river estuary and the northern south China Sea shelf. *Geochimica Cosmochimica Acta* 282, 324–339. doi: 10.1016/j.gca.2020.04.032

Willey, J. D. (1974). The effect of pressure on the solubility of amorphous silica in seawater at 0 c. *Mar. Chem.* 2 (4), 239–250. doi: 10.1016/0304-4203(74)90018-8

Wu, B., and Liu, S. M. (2020). Dissolution kinetics of biogenic silica and the recalculated silicon balance of the East China Sea. *Sci. Total Environ.* 743, 140552. doi: 10.1016/j.scitotenv.2020.140552

Wu, B., Liu, S. M., and Ren, J. L. (2017). Dissolution kinetics of biogenic silica and tentative silicon balance in the yellow Sea. *Limnology Oceanography* 62 (4), 1512–1525. doi: 10.1002/lno.10514

Wu, B., Lu, C., and Liu, S. (2015). Dynamics of biogenic silica dissolution in jiaozhou bay, western yellow Sea. *Mar. Chem.* 174, 58–66. doi: 10.1016/j.marchem.2015.05.004

Xiao, W., Wang, L., Laws, E., Xie, Y., Chen, J., Liu, X., et al. (2018). Realized niches explain spatial gradients in seasonal abundance of phytoplankton groups in the south China Sea. *Prog. Oceanography* 162, 223–239. doi: 10.1016/j.pocean.2018.03.008

Yang, B., Liu, S.-M., and Zhang, G.-L. (2018). Geochemical characteristics of phosphorus in surface sediments from the continental shelf region of the northern south China Sea. *Mar. Chem.* 198, 44–55. doi: 10.1016/j.marchem.2017.11.001

Zhang, X., Ren, J., Guo, Y., Li, L., and Zhang, R. (2020). Distributions and influencing factors of dissolved aluminum in the zhujiang river estuary,continental slope of the northern south China Sea in autumn and summer. *Haiyang Xuebao* 42 (02), 10–21. (in Chinese with English abstract)

Zhang, L. L., Wang, R. J., Chen, M. H., Liu, J. G., Zeng, L. L., Xiang, R., et al. (2015). Biogenic silica in surface sediments of the south China Sea: Controlling factors and paleoenvironmental implications. *Deep-Sea Res. Part Ii-Topical Stud. Oceanography* 122, 142–152. doi: 10.1016/j.dsr2.2015.11.008

Zhou, P., Li, D., Liu, G., Men, W., and Ji, L. (2010). Biogenic silica in surface sediments of the northeastern and southern south China Sea. *J. Trop. Oceanography* 29 (04), 40–47. (in Chinese with English abstract)